Research Square

Preprints are preliminary reports that have not undergone peer review.
They should not be considered conclusive, used to inform clinical practice,
or referenced by the media as validated information.

Hyperglycaemia-Induced Impairment of the Autorhythmicity and Gap Junction Activity of Mouse Embryonic Stem Cell-Derived Cardiomyocyte-Like Cells

Amanda Menzele
University of Cape Town
Hamida Aboalgasm
University of Cape Town
Robea Ballo
University of Cape Town
Asfree Gwanyanya (asfree.gwanyanya@uct.ac.za)
University of Cape Town

Research Article

Keywords: cardiomyocyte, hyperglycaemia, stem cell, autorhythmicity, gap junction, transforming growth factor

Posted Date: July 19th, 2022

DOI: https://doi.org/10.21203/rs.3.rs-1832538/v1

License: This work is licensed under a Creative Commons Attribution 4.0 International License.
Read Full License

Abstract

Diabetes mellitus with hyperglycaemia is a major risk factor for malignant cardiac dysrhythmias. However, the underlying mechanisms remain unclear, especially during the embryonic developmental phase of the heart. This study investigated the effect of hyperglycaemia on the pulsatile activity of stem cell-derived cardiomyocytes. Mouse embryonic stem cells (mESCs) were differentiated into cardiac-like cells through embryoid body (EB) formation, in either baseline glucose or high glucose conditions. Action potentials (APs) were recorded using a voltage-sensitive fluorescent dye and gap junction activity was evaluated using scrape-loading lucifer yellow dye transfer assay. Molecular components were detected using immunocytochemistry and immunoblot analyses. High glucose decreased the spontaneous beating rate of EBs and shortened the duration of onset of quinidine-induced asystole. Furthermore, it altered AP amplitude, but not AP duration, and had no impact on the expression of the hyperpolarisation-activated cyclic nucleotide-gated isoform 4 (HCN4) channel nor on the EB beating rate response to ivabradine nor isoprenaline. High glucose also decreased both the intercellular spread of lucifer yellow within an EB and the expression of the cardiac gap junction protein connexin 43 as well as upregulated the expression of transforming growth factor beta 1 (TGFβ1) and phosphorylated Smad3. High glucose suppressed the autorhythmicity and gap junction conduction of mESC-derived cardiomyocytes, via mechanisms probably involving TGFβ1/Smad3 signalling. The results allude to glucotoxicity related proarrhythmic effects, with potential clinical implications in foetal diabetic cardiac disease.

Introduction

Cardiovascular complications of diabetes mellitus with inadequately controlled hyperglycaemia are a major cause of death in both adults and children [1, 2]. Children, in particular offspring of diabetic mothers, are at a great risk of developing life-long complications such as cardiomyopathy and malignant dysrhythmias [3, 4]. Furthermore, foetal and neonatal dysrhythmias as a result of maternal gestational diabetes are more prevalent than generally reported [5], partly because, unlike cardiac structural defects, dysrhythmias are not readily diagnosed and not often investigated [6].

Dysrhythmias in foetal diabetic conditions occur through a maladaptive pathological electrical remodelling of the foetal heart in response to hyperglycaemia and other diabetic metabolic abnormalities [7–9], but the mechanisms remain unclear. Although such foetal cardiac complications persist and progress in later life, they are often only detected when other super-added features of diabetes such as myocardial infarction and heart failure become apparent [10]. In adult hearts, a key process in diabetic cardiac remodelling is the re-activation of the foetal gene programme to try to induce cardiomyocyte proliferation and replace damaged cells [11, 12]. However, adult hearts differ from those of foetuses in that cardiomyocytes exit the cell cycle at birth [13], and therefore adult cells lose the capacity to proliferate and repair optimally during diabetic remodelling [14, 15]. As such, there is limited knowledge on therapeutic interventions for diabetic foetal cardiac diseases, since the cardiac developmental pathophysiology is not fully understood.

We previously established and characterised a stem cell-derived cardiac cellular model that mimics cardiac cellular development, and showed that hyperglycaemia suppressed the cardiac differentiation of mouse embryonic stem cells (mESCs) and induced cardiomyocyte contractile dysfunction, features that were attributed to oxidative stress and apoptosis [16, 17]. However, the effect of hyperglycaemia on the spontaneous beating characteristics of those cardiac-like cells remains unclear. In the present study, we used the mESC-derived cardiac cellular hyperglycaemic model to study effects on autorhythmicity and gap junction function, and explored the possible underlying mechanisms.

Materials And Methods

Stem Cell Proliferation and Cardiac Differentiation

Cell culture materials were obtained from ThermoFisher Scientific (LTC Tech, South Africa), unless stated otherwise. Pluripotent mouse embryonic stem cells (mESCs) of the OLA 129 mouse cell line (gifted by Prof. F. Brombacher, University of Cape Town) were used as previously described [16, 17]. In short, undifferentiated mESCs were cultured on a mitomycin C inactivated mouse embryonic fibroblast (iMEF) feeder cell layer on 0.1% gelatin-coated culture dishes under standardised conditions (humidified 5% CO_2 at 37°C). The culture medium consisted of Dulbecco's modified Eagles medium (DMEM)/4.5 g/l (i.e., 25 mM) glucose, supplemented with 15% foetal bovine serum (FBS), 1% glutamax, 1% penicillin/streptomycin, 0.1% βmercaptoethanol, and 5 ng/ml leukaemia inhibitory factor (LIF; #A35933, ThermoFisher Scientific). Cells were passaged 2–3 times onto new iMEF layers at 70–80% confluency using dispase protease solution (5 mg/ml; Sigma, SA).

The mESCs were differentiated into cardiomyocyte-like cells using the hanging drop method and embryoid body (EB) formation as previously described [17]. Briefly, to form an EB, a fixed number of mESCs (1000 cells; dissociated from the iMEF feeder layer) were seeded into 20 µl of LIF-free differentiation medium [18, 19] containing DMEM/25 mM glucose, supplemented with 10% FBS, 1% glutamax, 1% penicillin/streptomycin, and 0.1% βmercaptoethanol. EBs were expanded further in suspension culture and thereafter plated onto 0.1% gelatin-coated coverslips or glass-bottomed imaging dishes for further culture. The first day of the hanging drop protocol was taken as day one of the differentiation protocol.

Experimental Treatments

The mESCs were differentiated in DMEM medium containing either the baseline (25 mM) glucose [20–22] or high (50 mM) glucose [23, 24] as previously described [16, 17], from day one of the differentiation protocol. Osmolality changes due to glucose addition were not adjusted for, as in other *in vitro* studies [16, 17, 23, 24], and so as to mimic *in vivo* diabetic hyperglycaemia with uncorrected osmolarity changes. Measurements on EBs on coverslips and EB sample collection were performed after approximately two weeks (day 1719) of the differentiation protocol. Each test drug (dissolved in water) ivabradine (10 µM), isoprenaline (12 mM), or quinidine (1 µM) was applied in the culture medium under standard conditions. Still images and time-lapse images of beating EBs were captured on an EVOS™ M5000 imaging system

(ThermoFisher Scientific). Images were analysed with ImageJ (NIH, USA) and a motion-detecting macro Myocyter™ [25], which produces a graphical output of the amplitude of cellular contraction of over time.

Action Potential Measurements

Action potentials (APs) were recorded using a voltage-sensitive fluorescent dye di4ANEPPS (#D1199, ThermoFisher Scientific). EBs (plated on gelatin-coated glass-bottomed imaging dishes) were loaded with 10-μM di-4-ANEPPS (dissolved in DMSO) in the culture medium and incubated for 15–20 minutes and mounted in an incubation chamber (5% CO_2 at 37 ℃) on the stage of a Carl Zeiss LSM880 Airyscan™ confocal microscope for imaging using the ZEN software (Zeiss.com). Fluorescent signals were analysed with ImageJ (NIH, USA) using the LC_Pro Plugin [26], from which AP amplitude and AP duration at 50% repolarisation (APD_{50}) and at 90% repolarisation (APD_{90}) were quantified as the averaged data of APs recorded over 6 seconds. The relative fluorescence intensity was expressed as fluorescence (F) normalised to the baseline fluorescence (F_0).

Scrape-Loading Dye Transfer Assay

The scrape-loading dye transfer assay adapted from [27] was used to assess gap-junction intercellular communication within an EB. A clean linear cut was made across an individual EB plated on a glass coverslip using a curved surgical scalpel blade. The EB was then loaded with lucifer yellow fluorescent dye added into the culture medium (1 mg/ml, dissolved in water; Sigma, SA) and incubated for 5 minutes under standard culture conditions. The EB on the coverslip was rinsed, fixed with 10% formalin solution, and imaged on the EVOS™ M5000 fluorescence microscope. The distance of lucifer yellow dye spread was analysed using ImageJ (NIH, USA).

Immunocytochemistry

Immunocytochemistry was performed on adherent EBs as previously described [16, 17]. Samples were fixed with 4% paraformaldehyde, permeabilized with ice-cold methanol, and blocked using 3% bovine serum albumin (BSA) with 0.01% Triton X100 in phosphate-buffered saline (PBS). Samples were incubated overnight (at 4 ^{o}C in PBS with 1% BSA) with primary antibodies directed against α-actinin 2 (dilution 1:250; #701914, ThermoFisher Scientific) or connexin 43 (dilution 1:200; #138300, ThermoFisher Scientific). The samples were then incubated with a fluorophore-conjugated secondary antibody (Alexa Fluor 488, dilution 1:5000; #715-546-150, Amersham or Cy3, dilution 1:1000; #711-166-152, Amersham) for 2 hours at room temperature. The samples were counterstained with Hoechst 33258 (0.5 μg/ml; Sigma, SA) and imaged on a Carl Zeiss LSM880 Airyscan™ confocal microscope (magnification 40x) using ZEN software. Images were analysed using ImageJ (NIH, USA).

Western Blot

Western blot analysis was performed on homogenised EB samples as previously described [17]. Briefly, 30 μg of protein samples were electrophoresed on 10% sodium dodecyl sulphate-polyacrylamide gels (Mini-PROTEAN® Tetra Cell, BioRad, SA) and transferred to polyvinylidene fluoride membranes (Trans-Blot® Turbo™ Transfer System, Bio-Rad, SA). Membranes were blocked with 5% non-fat milk in 0.1%

Tween20 PBS (or with 3% BSA in 0.1% Tween20 tris-buffered saline for phosphorylated Smad3) for 1 hour at room temperature and incubated (overnight at 4°C) with a primary antibody (each from ThermoFisher Scientific) directed against either the hyperpolarisation-activated cyclic nucleotide-gated (HCN4) channel (dilution 1:500; #MA3903), connexin 43 (dilution 1:500; #138300), transforming growth factor beta 1 (TGF-β1; dilution 1:1000; #MA5-16949), or phosphorylated Smad3 (dilution 1:250; #44246G). β-actin (dilution 1:5000; #MA5-15739, ThermoFisher Scientific) or α-tubulin (dilution 1:3000; #ab15246, Abcam) was used as a loading control. The membranes were incubated with horseradish peroxidase (HRP)-conjugated secondary antibody (dilution 1:500; #6721, Abcam), and bands were detected on the X-ray film using enhanced chemiluminescence substrate (#170–5060, BioRad, SA). Images were analysed using ImageJ (NIH, USA).

Data Analysis

Data are expressed as box plot and the mean, and *n* indicates the number of EBs studied. Statistical analysis was conducted using Statistica (version 13). A Shapiro-Wilk test for normality was used to test the distribution of variables. For parametric data, an unpaired *t*test was used to compare differences between glucose groups, whereas a MannWhitney *U* test was used for non-parametric data. A value of $p \leq 0.05$ was considered statistically significant.

Results

Stem Cell Cardiac Differentiation and Effect of Hyperglycaemia on Beating Characteristics

Differentiated mESCs formed distinct, spherically-shaped spontaneously beating EBs (Fig. 1a). The EBs were made up of cells that stained positively for the cardiac sarcomeric protein α-actinin 2, which showed a typical striated pattern (Fig. 1b). The EB pulsatile activity, shown as a graphical output of the Myocyter™ [25] programme, had distinct peaks and troughs, with identifiable beat-to-beat intervals (Fig. 1c). A high glucose concentration in the culture medium decreased the EB beating rate ($p = 0.005$ *versus* baseline glucose; Fig. 1d). However, high glucose did not alter the standard deviation of the beat-to-beat interval ($p = 0.23$ *versus* baseline glucose; Fig. 1e), which is an indicator of the intrinsic variability of cellular pacemaker activity attributed to fluctuations in the baseline transmembrane potential [28]. The application of quinidine (1 μM) induced asystole significantly quicker in EBs cultured under high glucose compared to those in baseline glucose ($p = 0.040$; Fig. 1f).

We further evaluated the sensitivity of EBs to either an inhibitor of the cardiac pacemaker HCN channel ivabradine [29] or the adrenergic receptor/cAMP-mediated pacemaker channel stimulant isoprenaline [30]. High glucose had no significant effect on the extent of neither the 10-μM ivabradine-induced decrease in the EB beating rate nor the 12mM isoprenaline-induced increase in beating rate ($p > 0.05$ *versus* baseline glucose for each drug; Fig. 2a, b). Furthermore, immunoblot analysis showed no

significant difference in the expression of the main HCN channel isoform found in the sinoatrial node HCN4 [31] between the two glucose groups ($p = 0.61$; Fig. 2c, d).

Action Potentials (APs)

Given that hyperglycaemia moderately reduced (rather than abolish) the EB pulsatile activity, we hypothesised that hyperglycaemia induced defects in the generation or conduction of electrical activity in otherwise viable cells. For APs, the fluorescence signals emitted by a voltage-sensitive dye (di-4-ANEPPS) in EBs of both glucose groups typically showed AP waveforms with rapid depolarisation and repolarisation phases, without a noticeable plateau phase (Fig. 3a, b). The AP amplitude was significantly larger in high glucose conditions compared to baseline glucose ($p = 0.007$; Fig. 3c). However, there was no significant difference in the APD_{90}/APD_{50} ratio, which is the ratio of the AP duration (APD) at 50% repolarisation (APD_{50}) to the APD at 90% repolarisation (APD_{90}) ($p = 0.41$; Fig. 3d).

Gap Junction Conduction

Although there was no significant difference in the size of the beating area in EBs cultured in high glucose compared to those in baseline glucose ($p = 0.59$; Fig. 4a, b), high glucose significantly decreased the distance of the spread of lucifer yellow within an EB ($p = 0.014$ *versus* baseline glucose; Fig. 4c, d). Furthermore, qualitatively, there was a decrease in the expression of the major cardiac gap junction protein connexin 43, since connexin 43 was detected by immunocytochemistry only in two out of five EBs in high glucose conditions, whereas the protein could be detected in all seven EBs in baseline glucose conditions (Fig. 4e). Nonetheless, similar to the EBs in baseline glucose conditions, the EBs in high glucose that lacked connexin 43 still stained positively for the cardiac sarcomeric protein αactinin 2 (Fig. 4e). Similarly, immunoblot analysis showed a significant reduction in the expression of connexin 43 protein by high glucose ($p = 0.03$ *versus* baseline glucose; Fig. 4f, g).

Modulation of the Transforming Growth Factor Beta 1 (TGF-β1) Pathway

We further investigated the effect of hyperglycaemia on TGF-β1, a cytokine-like growth factor that is implicated in the pathological cardiac remodelling that involves the disruption of the cardiac conduction system [32, 33]. Western blot analysis showed that high glucose upregulated the expression of TGF-β1, relative to that of the housekeeping protein α-tubulin ($p = 0.04$ *versus* baseline glucose; Fig. 5a, c). In addition, high glucose significantly increased the expression (relative to β-actin) of phosphorylated Smad3, a TGF-β1 downstream pathway signalling molecule ($p = 0.02$ *versus* baseline glucose; Fig. 5b, d).

Discussion

In this study, hyperglycaemia decreased the spontaneous beating rate of mESC-derived cardiac-like cells, a result consistent with the autorhythmic defects in diabetic adult hearts [34–36] and in other mESC-derived cardiac-like cells [37]. However, the altered beating rate was unrelated to cellular beat-to-beat variability (Fig. 1e), which is proposed to reflect intrinsic fluctuations in the baseline transmembrane

potential within pacemaker tissue [28] and has been shown to be present in mESC-derived cardiomyocytes [38]. In animal studies, pacemaker cells isolated from diabetic rat hearts showed large fluctuations in the beat-to-beat intervals that manifested clinically as arrhythmias [39, 40]. Furthermore, in the present study, the decreased beating rate in high glucose seemed to be unrelated to changes in pacemaker channel sensitivity, since there was no significant difference in the expression of the main HCN channel isoform in the sinoatrial node HCN4 [31] nor in the modulation of HCN channels by either ivabradine [29] or isoprenaline [30]. These findings contrast with results in an animal study in which pacemaker tissue isolated from diabetic rats showed a diminished response to ivabradine [41].

In the present study, hyperglycaemia increased the sensitivity of EBs to quinidine as was evidenced by a quicker onset of the drug-induced asystole. Given that, among its actions, quinidine prominently blocks voltage-gated Na^+ channels [42], the high glucose effect could reflect an altered Na^+ channel sensitivity, but the role of the channel was not further evaluated in this study. Electrophysiologically, high glucose increased the AP amplitude, but not the AP duration. In contrast to the present findings, diabetic adult rat pacemaker tissue generally show decreased AP amplitude and prolonged AP duration [34, 43–45], features attributed to the downregulation of several ion channels contributing to the AP [46, 47]. As such, the differences between the AP results in the present study and those in the other studies could reflect the unique differences in the glucose sensitivity in developing cells *versus* adult cardiac cells. However, the reason for the increased AP amplitude observed in the present study is still unclear. A possible explanation could be a change in the resting membrane potential; however, in the present study, a voltage-sensitive dye was used to record APs (which has a limitation in that it only detects the relative changes in depolarisation or depolarisation), so the absolute resting potential could not be determined. Alternatively, there could be a change in the depolarising currents such as the voltage-gated Na^+ current, given the above-mentioned altered quinidine sensitivity. Finally, because of the downregulation of repolarising K^+ currents reported in diabetes [47], the unopposed depolarising AP upstroke currents could produce a greater AP overshoot. Taken together, the reduced EB beating rate, increased quinidine sensitivity, and altered AP amplitude indicate a propensity for dysrhythmias.

The reduction in lucifer yellow dye transfer and the downregulation of the expression of connexin 43 channels (without altering the size of the beating area), observed in the present study, indicate intercellular conduction defects consistent with the hyperglycaemic cell structural disruption previously observed in the same model [16]. The downregulation of connexin 43 has also been reported in cultured H9C2 cells exposed to high glucose [23], and in the rat diabetic heart (Zhang et al. 2019). Notably, the disruption of gap junctions could, in part, also account for the beating rate disturbances seen in this study, since connexins are proposed to mediate impulses within the pacemaker tissue itself, as part of the impulse generation process [46, 48].

Mechanistically, in the present study, hyperglycaemia upregulated the expression of TGF-β1 and phosphorylated Smad3, a TGF-β1 downstream signalling protein. The finding is consistent with that in diabetic rat hearts in which the TGF-β1/Smad3 pathway was also activated in inducing fibrosis [49], and suggests that the pathway could play a key role in the high glucose effects observed in the present study.

In diabetic hearts, TGF-β1 is known to be involved in the remodelling of cardiac conduction tissue, via the induction of interstitial fibrosis [44] or cardiomyocyte hypertrophy, with altered transcellular axial electrical resistance [50]. However, the mechanisms underlying TGF-β1-mediated effects seen in the present study require further investigations.

Limitations of this study include the clinical relevance of the unphysiologically high glucose (50 mM), which although suitable for an *in vitro* model (where the standard baseline glucose is supraphysiological, e.g., 25 mM), needs further validation in an *in vivo* model. Furthermore, although the heterogeneity of EBs was minimised by fixing the number of mESCs seeded into each hanging drop [18, 19], the EB may contain other active non-cardiac cells, of which the nature was not determined.

In conclusion, hyperglycaemia suppressed the autorhythmicity and gap junction function of mESC-derived cardiac-like cells, probably via the TGFβ1/Smad3 pathway. The results suggest that hyperglycaemia induces unique proarrhythmic effects in the developing cardiac cells, with potential clinical implications in foetal diabetic cardiac disease.

Declarations

Acknowledgements

The authors thank Desiree Bowers and Thulisa Mkatazo for tissue culture technical assistance.

Funding The study was funded by the South African Medical Research Council (MRC Grant Number 29841). A.M. was supported by the National Research Foundation of South Africa (NRF) Freestanding Scholarship.

Competing Interests The authors declare that they have no conflict of interest.

Data Availability Data and material available upon request.

Author Contribution A.G. and R.B. conceived and designed the study. A.M. and H.A. collected data. A.G. drafted the manuscript. All authors analysed data and critically revised the manuscript.

References

1. Dal Canto, E., Ceriello, A., Ryden, L., Ferrini, M., Hansen, T. B., Schnell, O., et al. (2019). Diabetes as a cardiovascular risk factor: An overview of global trends of macro and micro vascular complications. European Journal of Preventive Cardiology, *26*, 25–32. https://doi.org/10.1177/2047487319878371
2. Schafer, M., Nadeau, K. J., & Reusch, J. E. B. (2020). Cardiovascular disease in young People with Type 1 Diabetes: Search for Cardiovascular Biomarkers. Journal of Diabetes and Its Complications, *34*, 107651. https://doi.org/10.1016/j.jdiacomp.2020.107651

3. Akbariasbagh, P., Shariat, M., Akbariasbagh, N., & Ebrahim, B. (2017). Cardiovascular Malformations in Infants of Diabetic Mothers: A Retrospective Case-Control Study. Acta Medica Iranica, *55*, 103–108.
4. Hoodbhoy, Z., Mohammed, N., Aslam, N., Fatima, U., Ashiqali, S., Rizvi, A., et al. (2019). Is the child at risk? Cardiovascular remodelling in children born to diabetic mothers. Cardiology in the Young, *29*, 467–474. https://doi.org/10.1017/S1047951119000040
5. Pike, J. I., Krishnan, A., Kaltman, J., & Donofrio, M. T. (2013). Fetal and neonatal atrial arrhythmias: an association with maternal diabetes and neonatal macrosomia. Prenatal Diagnosis, *33*, 1152–1157. https://doi.org/10.1002/pd.4210
6. Killen, S. A., Mouledoux, J. H., & Kavanaugh-McHugh, A. (2014). Pediatric prenatal diagnosis of congenital heart disease. Current Opinion in Pediatrics, *26*, 536–545. https://doi.org/10.1097/MOP.0000000000000136
7. Basu, M., & Garg, V. (2018). Maternal hyperglycemia and fetal cardiac development: Clinical impact and underlying mechanisms. Birth Defects Research, *110*, 1504–1516. https://doi.org/10.1002/bdr2.1435
8. Pedra, S. R., Smallhorn, J. F., Ryan, G., Chitayat, D., Taylor, G. P., Khan, R., et al. (2002). Fetal cardiomyopathies: pathogenic mechanisms, hemodynamic findings, and clinical outcome. Circulation, *106*, 585–591. https://doi.org/10.1161/01.cir.0000023900.58293.fe
9. Nakano, H., Fajardo, V. M., & Nakano, A. (2021). The role of glucose in physiological and pathological heart formation. Developmental Biology, *475*, 222–233. https://doi.org/10.1016/j.ydbio.2021.01.020
10. Mehta, A., Bhattacharya, S., Estep, J., & Faiman, C. (2020). Diabetes and Heart Failure: A Marriage of Inconvenience. Clinics in Geriatric Medicine, *36*, 447–455. https://doi.org/10.1016/j.cger.2020.04.005
11. Lipsett, D. B., Frisk, M., Aronsen, J. M., Norden, E. S., Buonarati, O. R., Cataliotti, A., et al. (2019). Cardiomyocyte substructure reverts to an immature phenotype during heart failure. The Journal of Physiology, *597*, 1833–1853. https://doi.org/10.1113/JP277273
12. Rosa, C. M., Xavier, N. P., Henrique Campos, D., Fernandes, A. A., Cezar, M. D., Martinez, P. F., et al. (2013). Diabetes mellitus activates fetal gene program and intensifies cardiac remodeling and oxidative stress in aged spontaneously hypertensive rats. Cardiovascular Diabetology, *12*, 152. https://doi.org/10.1186/1475-2840-12-152
13. Bergmann, O., Zdunek, S., Felker, A., Salehpour, M., Alkass, K., Bernard, S., et al. (2015). Dynamics of Cell Generation and Turnover in the Human Heart. Cell, *161*, 1566–1575. https://doi.org/10.1016/j.cell.2015.05.026
14. Foglia, M. J., & Poss, K. D. (2016). Building and re-building the heart by cardiomyocyte proliferation. Development, *143*, 729–740. https://doi.org/10.1242/dev.132910
15. Lazar, E., Sadek, H. A., & Bergmann, O. (2017). Cardiomyocyte renewal in the human heart: insights from the fall-out. European Heart Journal, *38*, 2333–2342. https://doi.org/10.1093/eurheartj/ehx343

16. Aboalgasm, H., Ballo, R., & Gwanyanya, A. (2021). Organisational alteration of cardiac myofilament proteins by hyperglycaemia in mouse embryonic stem cell-derived cardiomyocytes. Journal of Muscle Research and Cell Motility, *42*, 419–428. https://doi.org/10.1007/s10974-021-09607-9
17. Aboalgasm, H., Ballo, R., Mkatazo, T., & Gwanyanya, A. (2021). Hyperglycaemia-Induced Contractile Dysfunction and Apoptosis in Cardiomyocyte-Like Pulsatile Cells Derived from Mouse Embryonic Stem Cells. Cardiovascular Toxicology, *21*, 695–709. https://doi.org/10.1007/s12012-021-09660-3
18. Lee, M. Y., Cagavi Bozkulak, E., Schliffke, S., Amos, P. J., Ren, Y., Ge, X., et al. (2011). High density cultures of embryoid bodies enhanced cardiac differentiation of murine embryonic stem cells. Biochemical and Biophysical Research Communications, *416*, 51–57. https://doi.org/10.1016/j.bbrc.2011.10.140
19. Wobus, A. M., Guan, K., Yang, H. T., & Boheler, K. R. (2002). Embryonic stem cells as a model to study cardiac, skeletal muscle, and vascular smooth muscle cell differentiation. Methods in Molecular Biology, *185*, 127–156. https://doi.org/10.1385/1-59259-241-4:127
20. Ali, N. N., Xu, X., Brito-Martins, M., Poole-Wilson, P. A., Harding, S. E., & Fuller, S. J. (2004). Beta-adrenoceptor subtype dependence of chronotropy in mouse embryonic stem cell-derived cardiomyocytes. Basic Research in Cardiology, *99*, 382–391. https://doi.org/10.1007/s00395-004-0484-5
21. Crespo, F. L., Sobrado, V. R., Gomez, L., Cervera, A. M., & McCreath, K. J. (2010). Mitochondrial reactive oxygen species mediate cardiomyocyte formation from embryonic stem cells in high glucose. Stem Cells, *28*, 1132–1142. https://doi.org/10.1002/stem.441
22. Guan, K., Furst, D. O., & Wobus, A. M. (1999). Modulation of sarcomere organization during embryonic stem cell-derived cardiomyocyte differentiation. European Journal of Cell Biology, *78*, 813–823. https://doi.org/10.1016/S0171-9335(99)80032-6
23. Han, S. S., Wang, G., Jin, Y., Ma, Z. L., Jia, W. J., Wu, X., et al. (2015). Investigating the mechanism of hyperglycemia-induced fetal cardiac hypertrophy. PloS One, *10*, e0139141. https://doi.org/10.1371/journal.pone.0139141
24. Xu, X., Ruan, L., Tian, X., Pan, F., Yang, C., & Liu, G. (2020). Calcium inhibitor inhibits high glucose-induced hypertrophy of H9C2 cells. Molecular Medicine Reports, *22*, 1783–1792. https://doi.org/10.3892/mmr.2020.11275
25. Grune, T., Ott, C., Haseli, S., Hohn, A., & Jung, T. (2019). The "MYOCYTER" - Convert cellular and cardiac contractions into numbers with ImageJ. Scientific Reports, *9*, 15112. https://doi.org/10.1038/s41598-019-51676-x
26. Francis, M., Waldrup, J., Qian, X., & Taylor, M. S. (2014). Automated analysis of dynamic Ca^{2+} signals in image sequences. Journal of Visualized Experiments, e51560. https://doi.org/10.3791/51560
27. Babica, P., Sovadinova, I., & Upham, B. L. (2016). Scrape Loading/Dye Transfer Assay. Methods in Molecular Biology, *1437*, 133–144. https://doi.org/10.1007/978-1-4939-3664-9_9
28. Ponard, J. G., Kondratyev, A. A., & Kucera, J. P. (2007). Mechanisms of intrinsic beating variability in cardiac cell cultures and model pacemaker networks. Biophysical Journal, *92*, 3734–3752.

https://doi.org/10.1529/biophysj.106.091892

29. Thollon, C., Bedut, S., Villeneuve, N., Coge, F., Piffard, L., Guillaumin, J. P., et al. (2007). Use-dependent inhibition of hHCN4 by ivabradine and relationship with reduction in pacemaker activity. British Journal of Pharmacology, *150*, 37–46. https://doi.org/10.1038/sj.bjp.0706940
30. Bucchi, A., Baruscotti, M., Robinson, R. B., & DiFrancesco, D. (2003). I(f)-dependent modulation of pacemaker rate mediated by cAMP in the presence of ryanodine in rabbit sino-atrial node cells. Journal of Molecular and Cellular Cardiology, *35*, 905–913. https://doi.org/10.1016/s0022-2828(03)00150-0
31. Hennis, K., Biel, M., Fenske, S., & Wahl-Schott, C. (2022). Paradigm shift: new concepts for HCN4 function in cardiac pacemaking. Pflügers Archiv. European Journal of Physiology, *474*, 649–663. https://doi.org/10.1007/s00424-022-02698-4
32. Derangeon, M., Montnach, J., Cerpa, C. O., Jagu, B., Patin, J., Toumaniantz, G., et al. (2017). Transforming growth factor beta receptor inhibition prevents ventricular fibrosis in a mouse model of progressive cardiac conduction disease. Cardiovascular Research, *113*, 464–474. https://doi.org/10.1093/cvr/cvx026
33. Dzialo, E., Tkacz, K., & Blyszczuk, P. (2018). Crosstalk between the TGF-beta and WNT signalling pathways during cardiac fibrogenesis. Acta Biochimica Polonica, *65*, 341–349. https://doi.org/10.18388/abp.2018_2635
34. Howarth, F. C., Al-Sharhan, R., Al-Hammadi, A., & Qureshi, M. A. (2007). Effects of streptozotocin-induced diabetes on action potentials in the sinoatrial node compared with other regions of the rat heart. Molecular and Cellular Biochemistry, *300*, 39–46. https://doi.org/10.1007/s11010-006-9366-5
35. Malone, M. A., Schocken, D. D., Hanna, S. K., Liang, X., & Malone, J. I. (2007). Diabetes-induced bradycardia is an intrinsic metabolic defect reversed by carnitine. Metabolism, *56*, 1118–1123. https://doi.org/10.1016/j.metabol.2007.04.005
36. Zhang, Y., Wang, Y., Yanni, J., Qureshi, M. A., Logantha, S., Kassab, S., et al. (2019). Electrical Conduction System Remodeling in Streptozotocin-Induced Diabetes Mellitus Rat Heart. Frontiers in Physiology, *10*, 826. https://doi.org/10.3389/fphys.2019.00826
37. Yang, P., Chen, X., Kaushal, S., Reece, E. A., & Yang, P. (2016). High glucose suppresses embryonic stem cell differentiation into cardiomyocytes: High glucose inhibits ES cell cardiogenesis. Stem Cell Research & Therapy, *7*, 187. https://doi.org/10.1186/s13287-016-0446-5
38. Niehoff, J., Matzkies, M., Nguemo, F., Hescheler, J., & Reppel, M. (2016). Beat Rate Variability in Murine Embryonic Stem Cell-Derived Cardiomyocytes: Effect of Antiarrhythmic Drugs. Cellular Physiology and Biochemistry, *38*, 646–658. https://doi.org/10.1159/000438657
39. Albarado-Ibanez, A., Avelino-Cruz, J. E., Velasco, M., Torres-Jacome, J., & Hiriart, M. (2013). Metabolic syndrome remodels electrical activity of the sinoatrial node and produces arrhythmias in rats. PloS One, *8*, e76534. https://doi.org/10.1371/journal.pone.0076534
40. Soltysinska, E., Speerschneider, T., Winther, S. V., & Thomsen, M. B. (2014). Sinoatrial node dysfunction induces cardiac arrhythmias in diabetic mice. Cardiovascular Diabetology, *13*, 122.

https://doi.org/10.1186/s12933-014-0122-y

41. Huang, X., Zhong, N., Zhang, H., Ma, A., Yuan, Z., & Guo, N. (2017). Reduced expression of HCN channels in the sinoatrial node of streptozotocin-induced diabetic rats. Canadian Journal of Physiology and Pharmacology, *95*, 586–594. https://doi.org/10.1139/cjpp-2016-0418
42. Roden, D. M. (2014). Pharmacology and Toxicology of Nav1.5-Class 1 anti-arrhythmic drugs. Cardiac Electrophysiology Clinics, *6*, 695–704. https://doi.org/10.1016/j.ccep.2014.07.003
43. Gallego, M., Zayas-Arrabal, J., Alquiza, A., Apellaniz, B., & Casis, O. (2021). Electrical Features of the Diabetic Myocardium. Arrhythmic and Cardiovascular Safety Considerations in Diabetes. Frontiers in Pharmacology, *12*, 687256. https://doi.org/10.3389/fphar.2021.687256
44. Liu, C., Fu, H., Li, J., Yang, W., Cheng, L., Liu, T., et al. (2012). Hyperglycemia aggravates atrial interstitial fibrosis, ionic remodeling and vulnerability to atrial fibrillation in diabetic rabbits. Anadolu Kardiyoloji Dergisi. The Anatolian Journal of Cardiology, *12*, 543–550. https://doi.org/10.5152/akd.2012.188
45. Ozturk, N., Uslu, S., & Ozdemir, S. (2021). Diabetes-induced changes in cardiac voltage-gated ion channels. World Journal of Diabetes, *12*, 1–18. https://doi.org/10.4239/wjd.v12.i1.1
46. Ferdous, Z., Qureshi, M. A., Jayaprakash, P., Parekh, K., John, A., Oz, M., et al. (2016). Different Profile of mRNA Expression in Sinoatrial Node from Streptozotocin-Induced Diabetic Rat. PloS One, *11*, e0153934. https://doi.org/10.1371/journal.pone.0153934
47. Howarth, F. C., Qureshi, M. A., Jayaprakash, P., Parekh, K., Oz, M., Dobrzynski, H., et al. (2018). The Pattern of mRNA Expression Is Changed in Sinoatrial Node from Goto-Kakizaki Type 2 Diabetic Rat Heart. *Journal of Diabetes Research*, *2018*, 8454078. https://doi.org/10.1155/2018/8454078
48. Boyett, M. R., Inada, S., Yoo, S., Li, J., Liu, J., Tellez, J., et al. (2006). Connexins in the sinoatrial and atrioventricular nodes. Advances in Cardiology, *42*, 175–197. https://doi.org/10.1159/000092569
49. Jia, X., Xiao, C., Sheng, D., Yang, M., Cheng, Q., Wu, J., et al. (2020). TRPV4 mediates cardiac fibrosis via the TGF-beta1/Smad3 signaling pathway in diabetic rats. Cardiovascular Toxicology, *20*, 492–499. https://doi.org/10.1007/s12012-020-09572-8
50. Dobaczewski, M., Chen, W., & Frangogiannis, N. G. (2011). Transforming growth factor (TGF)-beta signaling in cardiac remodeling. Journal of Molecular and Cellular Cardiology, *51*, 600–606. https://doi.org/10.1016/j.yjmcc.2010.10.033

Figures

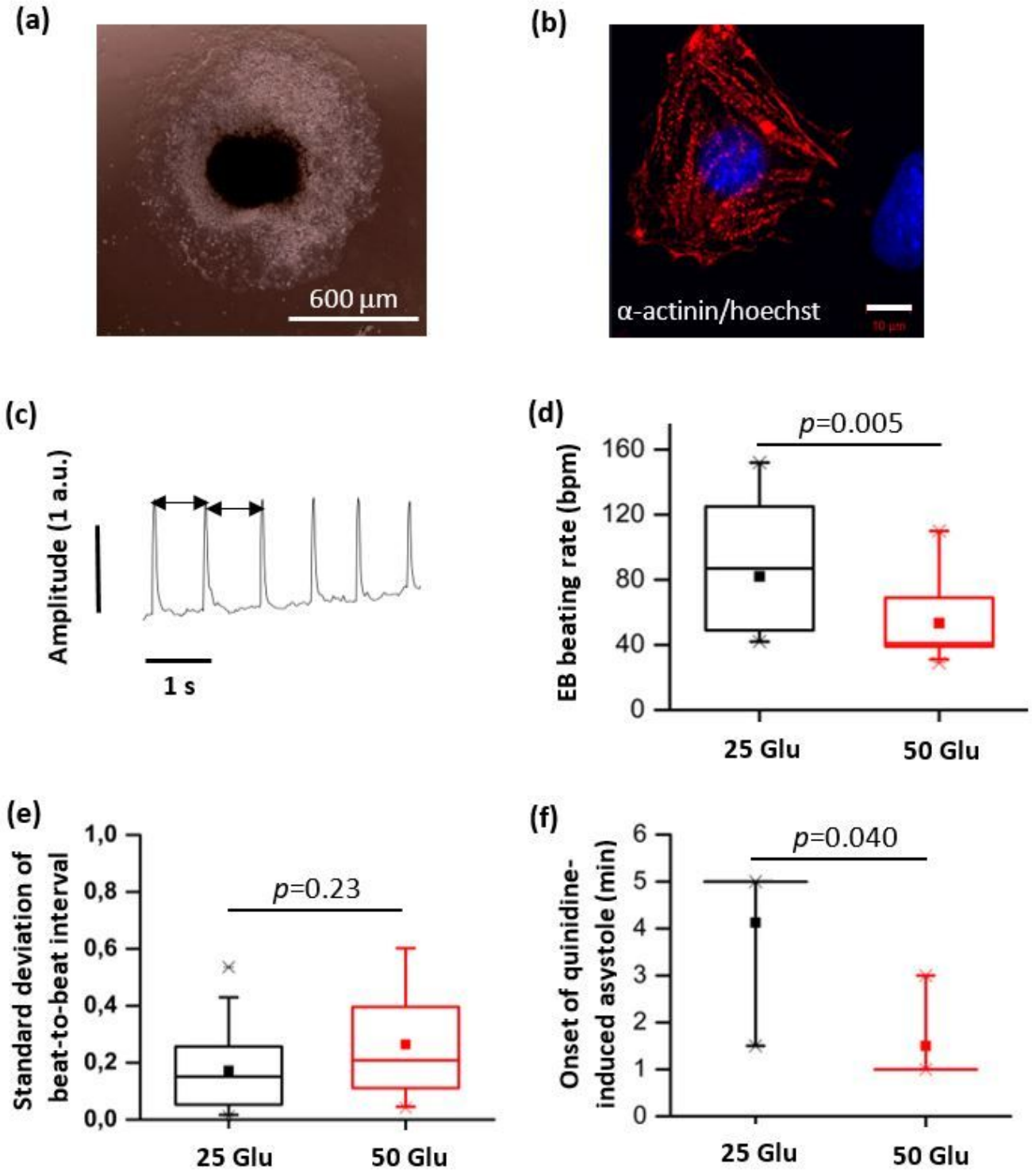

Figure 1

High glucose impairs embryoid body (EB) beating characteristics. **a** Representative light-microscopy image of an EB cultured under baseline (25 mM) glucose conditions (2x magnification; scale bar=600 µm). **b** Confocal microscopy merged image of a cell dissociated from an EB and stained with α-actinin 2 and Hoechst (40x magnification; scale bar=10 µm). **c** Representative tracing of an EB pulsatile activity (as detected by the Myocyterä programme), under baseline (25 mM) glucose conditions. Double arrow-

heads indicate the duration of beat-to-beat intervals of two consecutive beats. **d-f** Summary data (from 3 independent cell culture batches) of EB beating rate (*n*=20 EBs per group), the standard deviation of the EB beat-to-beat interval (*n*³20 EBs per group), and onset of 1-μM quinidine-induced asystole (*n*=4 EBs per group) under different glucose conditions. Data are shown as box plot and the mean (filled square). Glu, glucose; a.u., arbitrary unit

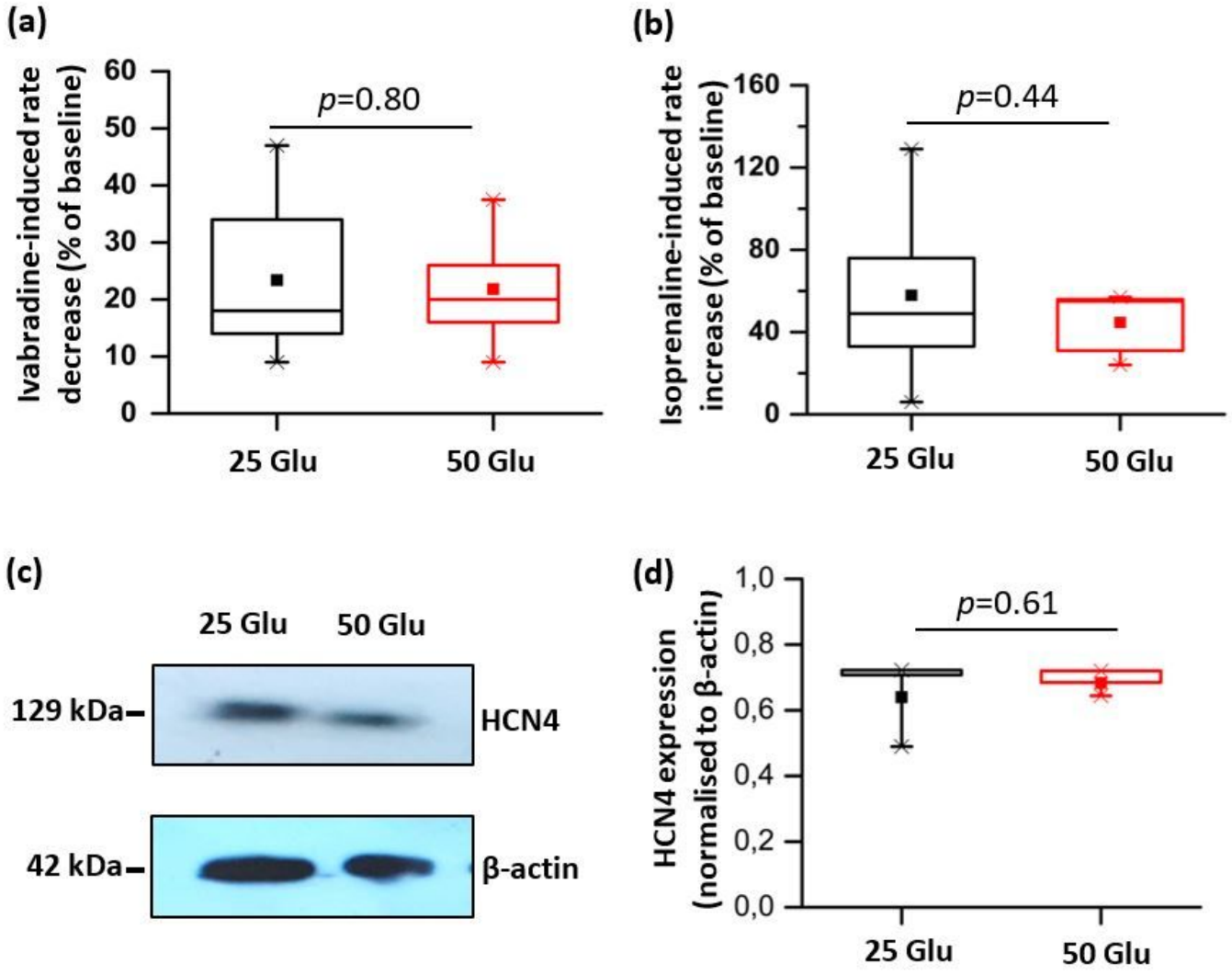

Figure 2

Effect of high glucose on pacemaker channel modulation. **a, b** Summary data of the percentage changes in EB beating rate induced by either ivabradine (10 μM; *n*=8 EBs per group, 2 independent cell culture batches) or isoprenaline (12 mM; *n*≥6 EBs per group, 2 independent cell culture batches). **c** Representative Western blot images of the hyperpolarization-activated cyclic nucleotide-gated isoform 4 (HCN4) channel protein and the housekeeping protein b-actin. **d** Summary data of HCN4 expression normalised to b-actin (*n*=3 replicates per group). Data are shown as box plot and the mean (filled square). Glu, glucose

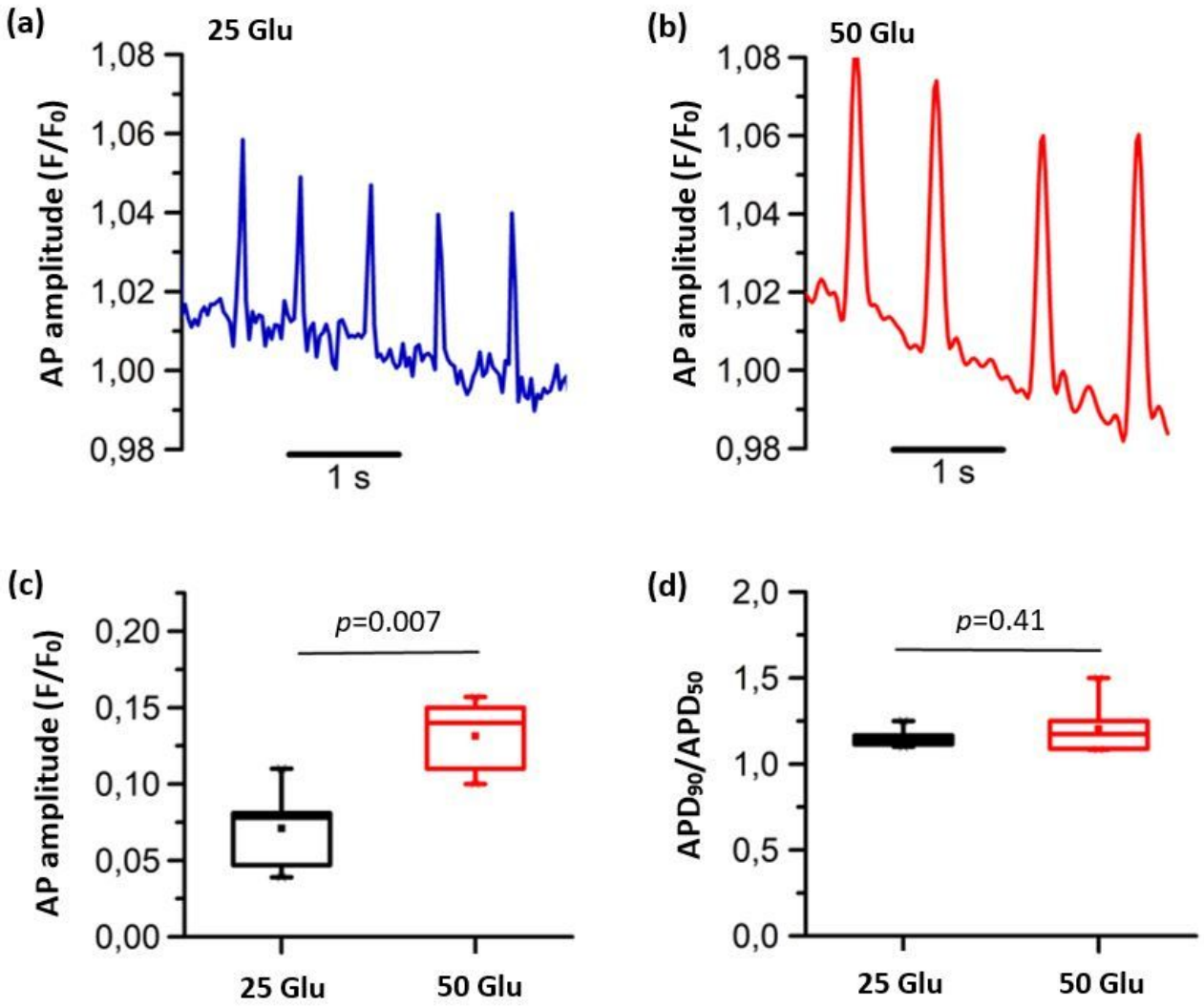

Figure 3

Effect of high glucose on action potentials. **a, b** Representative tracings of action potentials (AP) recorded using a voltage-sensitive fluorescent dye, di-4-ANEPPS. AP amplitude is expressed as fluorescence (F) normalised to the baseline fluorescence (F_0). **c, d** Summary data of AP amplitude and APD_{50}/APD_{90} (*n*=5 EBs per group). AP data were obtained using the LC_Pro programme, and although the baseline potential had some instabilities due to background noise, the signal-to-noise ratio was optimal for the detection of AP parameters. Data are shown as box plot and the mean (filled square). APD_{50} and APD_{90}, AP duration at 50% and 90% of repolarisation, respectively. Glu, glucose

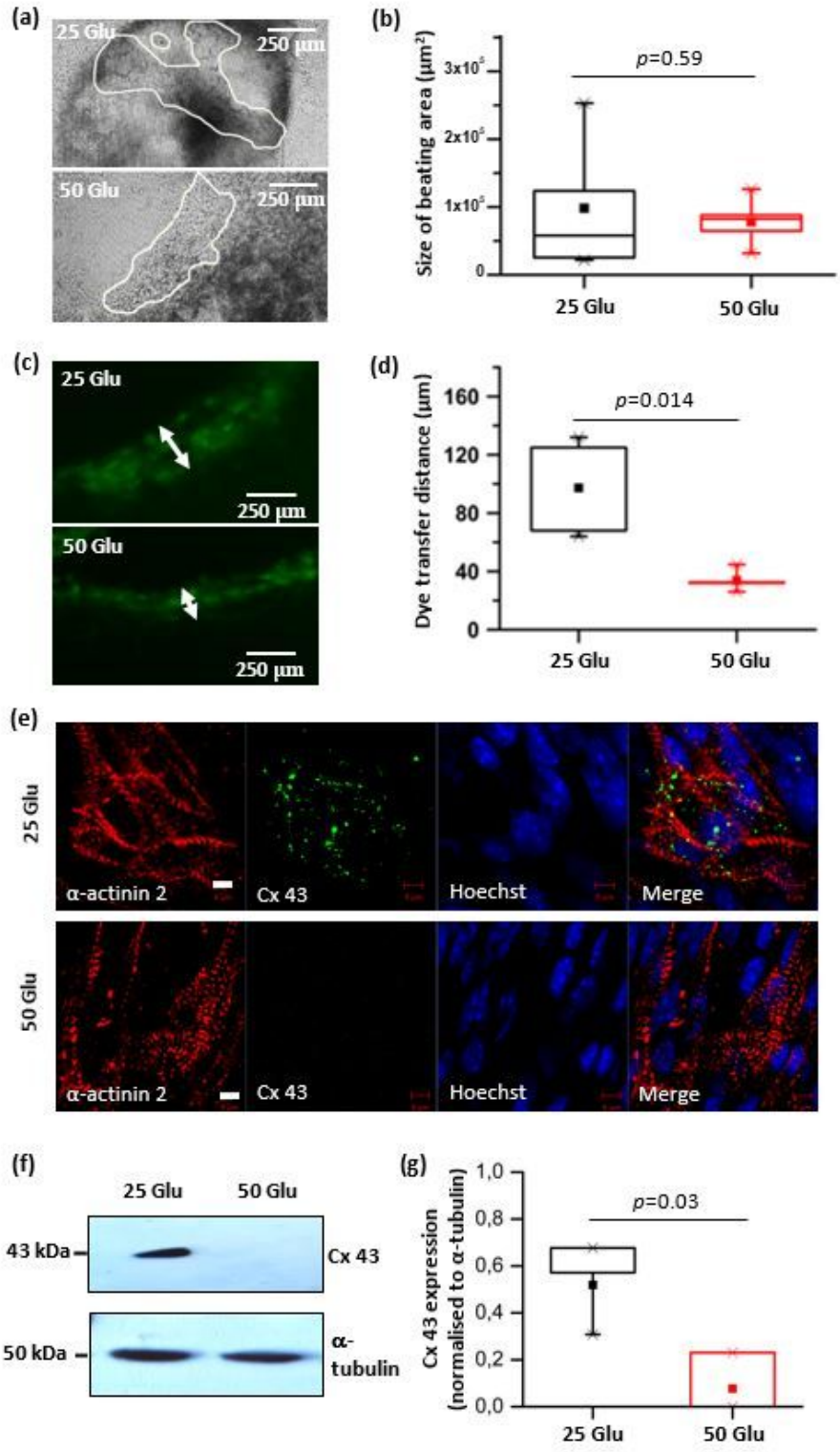

Figure 4

Effect of high glucose on gap junctions. a Light microscopy images of beating EBs, with the beating area outlined in white. **b** Summary data of size of EB beating area (*n*=8 EBs per group). **c** Lucifer yellow dye fluorescence signals in individual EBs, post scrape loading of the dye. Double arrowheads indicate distance of dye transfer. **d** Quantitative analysis of dye transfer distance (*n*=5 EBs per group, 3 independent cell culture batches). **e** Representative confocal microscopy images of α-actinin 2, connexin

43 (Cx 43), hoechst, and merged images. Scale bar=5 μm. Notice the lack of Cx 43 signal in high glucose (Cx 43 was detected in each of the 7 EBs under baseline glucose, but only in 2 out of 5 EBs in high glucose. **f** Representative Western blot images of Cx 43 and the housekeeping protein α-tubulin. **g** Summary data of Cx 43 expression normalised to α-tubulin (*n*=3 replicates per group). Data are shown as box plot and the mean (filled square). Glu, glucose

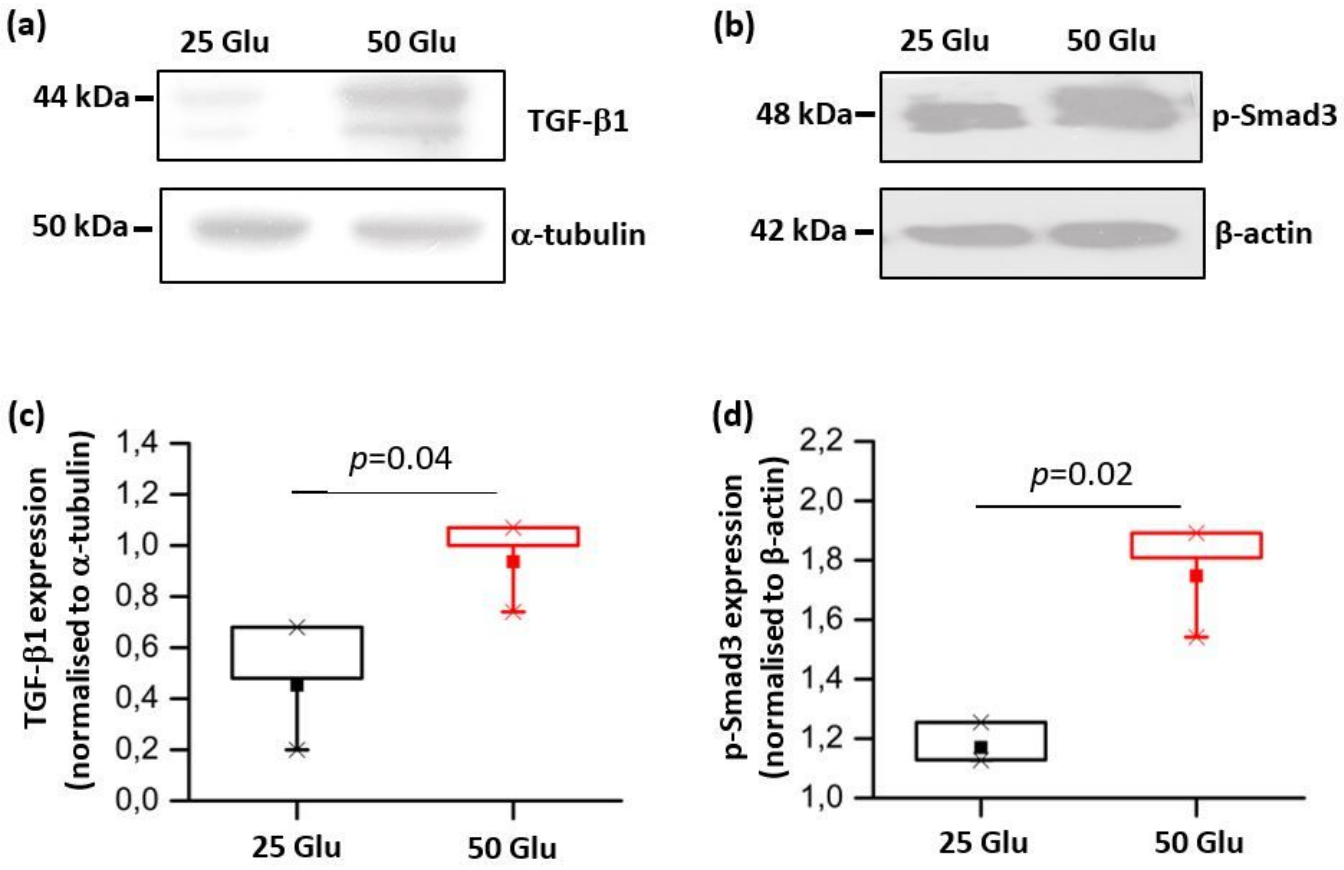

Figure 5

Effect of high glucose on the transforming growth factor beta 1 (TGF-β1) pathway. a, b Representative Western blot images of TGF-b1 and phosphorylated Smad3 (p-Smad3) and the housekeeping proteins a-tubulin and b-actin. **c, d** Summary data of TGF-b1 expression normalised to a-tubulin (*n*=3 replicates per group) and of p-Smad3 normalised to b-actin (*n*=3 replicates per group). Data are shown as box plot and the mean (filled square). Glu, glucose